Kinetic of colloidal-chemical transformations during the decomposition of ammonia complexes of Zn(II) in alkaline solutions

Maria A. Maksimova[1,a], Evgeny V. Polyakov[1,b], Ilya V. Volkov[1],
Aleksandr P. Tyutyunnik[1], Alexey A. Ioshin[1,c]

[1]ISSC UB RAS, Ekaterinburg, Russia

[a]msalimova1993@gmail.com, [b]polyakov@ihim.uran.ru, [c]aaioshin@yandex.ru

Corresponding author: Maria A. Maksimova, msalimova1993@gmail.com

ABSTRACT For the closed system (Σ): Zn^{2+}–$NH_{3,aq}$–$NH_{3,gas}$, H^+–OH^-–$N_{2,gas}$, experimental data on the change in the concentration of in the composition of the ammonia complex $Zn(NH_3)_4^{2+}$ in solution, colloidal particles $Zn(OH)_2$/ZnO in solution and growing film on the reactor walls are presented depending on the synthesis time, zinc concentration and synthesis temperature T_s in the range of 50 –99 °C. It has been established that up to 95 °C the ion-molecular growth of $Zn(OH)_2$/ZnO clusters in solution (Σ) proceeds in a diffusion-controlled mode of homogeneous growth until reaching of their critical size. Further growth of ther critical clusters is followed by aggregation and coalescence of critical sized clusters into microcrystals with the formation of a film on a glass substrate of various morphologies. The solubility of such a film is determined by the size of critical clusters, which preserves in the growing polycrystal in the form of coherent scattering region (CSR). With an increase in the synthesis temperature to 99 °C, the aggregation mechanism is replaced by a faster diffusion-controlled attachment of Zn (II) ammonia complex to the end surface of the growing microcrystals simultaneously in colloid solution and in the film.

KEYWORDS Zn(II), ammonia complex, $Zn(OH)_2$/ZnO, colloid, film, growth, mechanism

ACKNOWLEDGEMENTS The work was carried out with the support of the State Program of Fundamental Scientific Research of the Russian Federation (project No. 124020600007-8).

FOR CITATION Maksimova M.A., Polyakov E.V., Volkov I.V., Tyutyunnik A.P., Ioshin A.A. Kinetic of colloidal-chemical transformations during the decomposition of ammonia complexes of Zn(II) in alkaline solutions. *Nanosystems: Phys. Chem. Math.*, 2024, **15** (4), 498–509.

1. Introduction

The colloidal-chemical nature of laminar systems formation in the liquid phase (thin films, layers, coatings) was first studied systematically at the beginning of the last century [1]. That work was further developed under the general motto of "chemical bath deposition" (CBD) methods [2–5]. The interest of technologists in CBD methods is due to the relative simplicity of their implementation, cost-effectiveness, the ability to scale up the technique of applying thin films, layers, coatings on substrates without the use of expensive and special equipment, high temperatures and pressures. This method can also be used to produce thin films with controlled structure and morphology, such as nanocrystalline flowers, oriented nanowires, and nanoribbons. They are recommended for the manufacture of films formed by particles of any shape, such as flat, spherical, porous and tubular structures [2].

The disadvantage of the methods is their relatively low reproducibility compared to physical deposition methods. This limitation is eliminated by optimizing the growth parameters [6]. Among the diverse objects of film synthesis by CBD methods, chalcogenide films are in the first place [4,7]. In recent decades, the production of 1-D films of metal-oxide nanoscale compounds and semiconductors, such as ZnO, was of particular interest. Their synthesis makes it possible to create ultrafine wires and rods on inorganic and polymer substrates for use as elements of solar converters, electronic circuits, radiation shields, light concentrators, and radiation coolers [8–13]. The kinetics of growth of thin films of oxides and chalcogenides from aqueous and mixed water-organic solutions differs depending on whether the mechanism of homogeneous or heterogeneous growth (heteronucleation) prevails during their formation [2, 3, 5]. Hydroxides, oxides, chalcogenides of Zn(II) belong to the group of compounds prone to the formation of colloidal solutions at relatively low values of supersaturation for metal ions. Heteronucleation is thought to be the main mechanism of film growth for them [5, 14]. After the first experimental studies of the initial stage of the colloidal-chemical mechanism of semiconducting film growth, it became clear that chalcogenide film formation on untreated surfaces proceeds only if a metal hydroxide film has been preliminarily formed [15, 16]. For example, the initial stage of sulfide film growth includes the formation of nanoclusters of the future hydroxide phase in a supersaturated ammonia solution. Then the nanoclusters cover the surface

of the substrate. This stage is responsible for the observed induction period of growth of many sulfide films from ammonia solutions [16]. The hydroxide phase acts as a natural surface activator. Its subsequent ion-exchange interaction [15–17] with the sulfide ions of the solution ensures the chemical modification of hydroxide into sulfide and the heterogeneous growth of the latter. At the same time, colloidal particles are formed in the volume of the solution (clusters, [18]), and their distribution at the film – solution phases interface is governed by the mechanism of heteronucleation [1, 3, 5, 16].

According to the cluster theory of crystal growth in solution, the size of primary colloidal particles (r) determines the relative solubility of the growing crystals as Gibbs-Thomson relation [18, 19]

$$RT_s \ln \frac{a}{a_0} = \frac{\sigma \overline{V}}{r}, \tag{1}$$

where R, T_s, $\overline{V}$, σ, a, a_0 are respectively the universal gas constant (J/mol, K), the synthesis temperature (K), the molar volume of crystals (m^3/mol), the surface tension (J/m^2), the activity (concentration) of crystals in the supersaturated and equilibrium solution (mol/kg). If there are factors that impede the growth of nanocrystals in the volume of solution (large surface charge, phase transformations in the surface layer of the nanocrystals with the formation of a non-autonomous phase [20] etc.), their size may fluctuate near the critical cluster [18]. Further accumulation of critical clusters leads to a transition from a homogeneous to a heterogeneous growth mechanism.

The lack of experimental data on the initial stages of the colloidal-chemical process in aqueous-ammonia solutions with the participation of hydroxides determines the importance of studying the kinetics of thermal hydrolysis of ammonia complexes of d-metals as a significant element of the general mechanisms of oxide and chalcogenides film growth [21, 22]. Regardless of the type of organic ligand (urea, hexamethylenetetramine, mono-, di-, triethanolamine, dimethylamine, tetramethylammonium, etc.), the destruction of ammonia zinc complexes with increasing temperature leads to alkaline hydrolysis with the subsequent formation of a hydroxide/oxide phase [23–30].

The results of the thermodynamic analysis of the concentration and temperature regions of predominance of Zn(OH)$_2$–ZnO in the system (Σ): "Zn^{2+}–NH$_{3,aq}$–NH$_3$, gas, H$^+$–OH$^-$–N$_{2,gas}$, show [29, 30] that the formation of the solid phase begins at pH $> 6 - 7$ and depends on the temperature. The reactions in aqueous-ammonia solution with the participation of Zn(OH)$_2$–ZnO particles are characterized by the presence of some volatile components of (Σ) in both the gaseous and liquid phases (NH$_3$(a,g), H$_2$O(a,g)) (Fig. 1) and the in the state of nano- and microbubbles in solution. The topics of gas bubbles origin and methods of their detecting in electrolyte solution are under discussion up to now [31]. Among adequate methods used for gas nanoparticles size and surface charge monitoring in water solution are instrumental methods of dynamic light scattering (DLS) coupled with laser Doppler electrophoresis (LDE) [32]. In our previous research we used both DLS and LDE method with the help of a Zetasizer Nano ZS particle analyzer (Malvern Panalytical Ltd.).
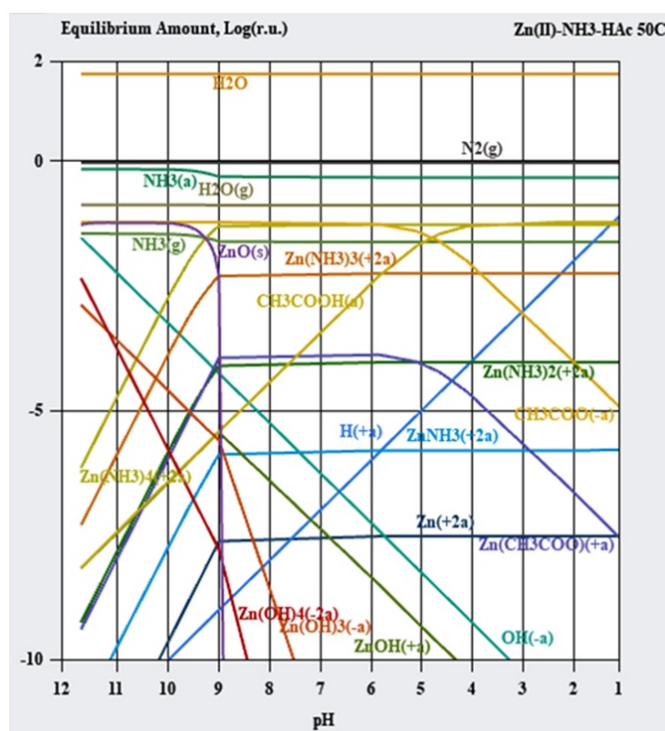
FIG. 1. Example of predominance diagram of chemical species in the system (Σ) at 50 $^\circ$C calculated with the help of HSC Chemistry 8 software

The growth of a hydroxide film on the surface of the substrate with the participation of gas bubbles at a relatively low temperature (less than 65 °C) gives a film with a $Zn(OH)_2$ (Wulfingit) structure and a foam-like morphology [29]. Above 80 °C, the films on the glass substrate acquire an orientation in the direction normal to the substrate surface, the hexagonal habit of ZnO (Wurtzite) and the morphology of drusen (nanoflowers) growing from a common center of crystallization, Fig. 2 and [22, 30, 33, 34]. The synthesis temperature also affects the ratio of $Zn(OH)_2$/ZnO phases in films, the optical width of the solid phase slit, and the luminescence intensity during the transition from $Zn(OH)_2$ to ZnO [35, 36].
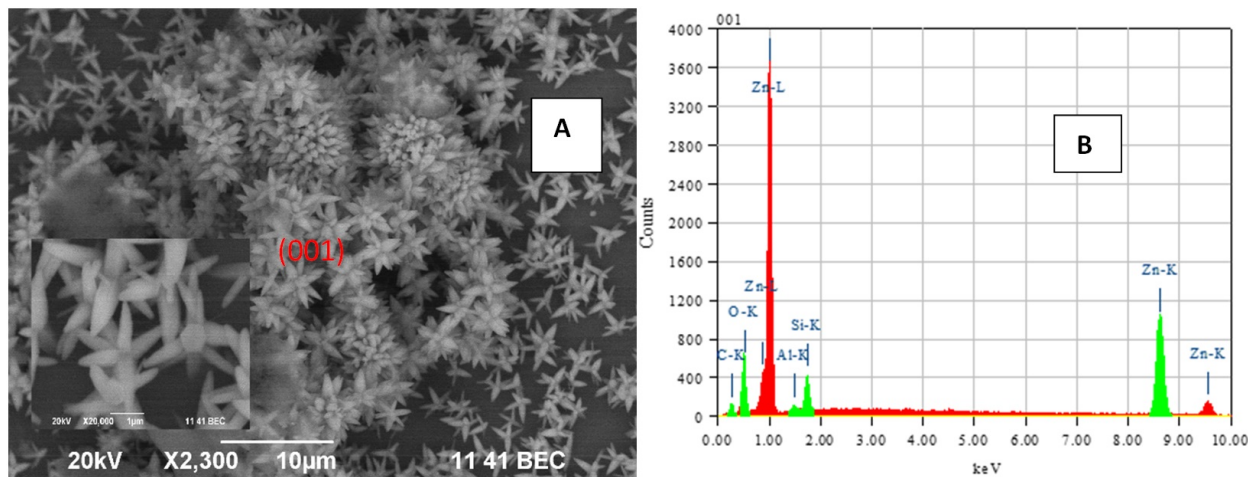
FIG. 2. (**A**) An example of the morphology of a ZnO film on a fragment of the glass wall of a test tube according to SEM data (enlarged fragment is shown in the inset). (**B**) X-ray fluorescence spectrum of ZnO particles at point (001). Synthesis duration 35 min, T_s = 85 °C

We have previously shown that the driving force behind the formation of $Zn(OH)_2$–ZnO nanoparticles in a closed initially homogeneous system (Σ) is the difference in the chemical potentials of ionic particles at 25 °C and at elevated synthesis temperature T_s (supersaturated system). By using the methods of vibrational spectroscopy, X-ray phase and chemical analysis, diffuse light scattering and electrophoresis we have established that the phase transition of $Zn(OH)_2$ to ZnO in the studied system occurs in the region of T_s = 85 – 90 °C, but at lower temperatures ZnO is also present in the solid as an impurity. The increase in the concentration of colloid and film, as well as in the electrical conductivity of the solution with the time of synthesis, obeys the equation of the 1st order irreversible reaction for zinc ions.

The transformation of ionic particles of $Zn(NH_3)_4^{2+}$ into colloidal microcrystals of the composition $Zn(OH)_2$–ZnO is a multistage process. The first stage takes place predominantly in the volume of the solution with the participation of the surfaces of the "gas bubbles-solution" interface as a result of rapid formation, growth and removal of gas bubbles from the solution during heating.

By comparing the variation in the size of colloid particles, their ζ-potential and ζ-potential of gas babbles in the solution as a function of reaction time we have concluded [29] that the interaction of positively charged $Zn(OH)_2$ nanoparticles with the negatively charged surface of gas bubbles may lead to the growth of colloidal aggregates "bubble||surface film" of hydroxide nanoparticles in the form of solid foam-like surface. Such morphology is seen on SEM pictures of films, synthesized at the induction stage of film growth.

After degassing of the electrolyte solution at the second stage of film formation, the morphology of the film changes drastically. On the SEM pictures we can see nucleation and growth of columnar microcrystals $Zn(OH)_2$–ZnO, which look like three-dimensional stars with conical spikes of hexagonal cross-section, Fig. 2. It is of interest to trace the relationship between the conditions of formation of nanocrystals as a result of thermal decomposition of the most stable complex $Zn(NH_3)_4^{2+}$ (or, more precisely, the ion pair $Zn(NH_3)_4(OH)_2$) and the parameters of colloidal aggregates in the volume of the solution and at the interface surfaces.

The aim of this work was to determine the kinetic regularities of the growth of $Zn(OH)_2$ films on the glass surface in thermally nonequilibrium alkaline ammonia solutions with the participation of the $Zn(NH_3)_4(OH)_2$ complex. We aimed also on establishing a relationship between the value of solubility of growing colloidal particles $Zn(OH)_2$–ZnO, the clusters of critical size in solution (hereinafter referred to as "critical clusters", r) according to equation (1), and the value of the coherent scattering region (CSR) in polycrystalline growth products according to X-ray phase analysis of $Zn(OH)_2$–ZnO films.

TABLE 1. The estimates of CSR sizes of the Wulfingit film by Williams–Hall method [37]. Temperature of the synthesis 50 °C, duration of the synthesis 80 min

Plane	Size, nm	Strain, 10^4	No. of reflections
All reflection	64.21	1.78	211
100	66.68	3.07	2
010	66.04	2.62	2
001	62.98	1.51	4
111	64.49	1.98	3

2. Experimental

To prepare a work solution, 4.39 g of $Zn(CH_3COO)_2 \times 2H_2O$ was dissolved in a small amount of water, 10 ml of concentrated ammonia was added and brought to a volume of 100 ml with deionized water (Millipore water treatment system). To adjust the pH to 10.2 – 10.3, 67 ml of NaOH solution with a concentration of 0.05 M was added drop by drop. The final volume of the obtained starting solution (167 ml) contained (mol/l) Zn(II)=0.12, NH3=1.0, NaOH=0.02. The kinetics of the synthesis of the $Zn(OH)_2$–ZnO colloid and the film was studied in a series of test tubes made of heat-resistant glass filled with a 5.0 ml work Zn(II) solution. The test tubes were closed with a rubber stopper. A Termex thermostat with water heat-carrier provided temperature stability and uniformity of the temperature field in the working area of the thermostat coolant, ± 1 °C. At specified time intervals, the corresponding test tube with the work solution was removed from the heat-carrier and the concentration of zinc was analyzed in the filtrate after acidifying the filtrate to a concentration of 1.8 – 2.0 mol/l with hydrochloric acid. The colloid part was separated from the solution by ultrafiltration through a double cellulose filter with a pore size of less than 100 nm under vacuum. The precipitate on the filter was sequentially dried and dissolved in 2 mol/l of hydrochloric acid (qualification "chemically pure") of a given volume. The mass of Zn(II) was determined in this volume by mass spectrometry with inductively coupled plasma and then the mass (mol) of metal in the form of a colloid in the system (Σ) under study was calculated at a given time. The zinc content in the film on the walls of the glass reactor was determined after dissolving the layer with hydrochloric acid of 2 mol/l in a volume equal to the volume of the solution under study (5.0 ml). The method of elemental analysis of solution, colloid, and film is described in more detail elsewhere [22, 24].
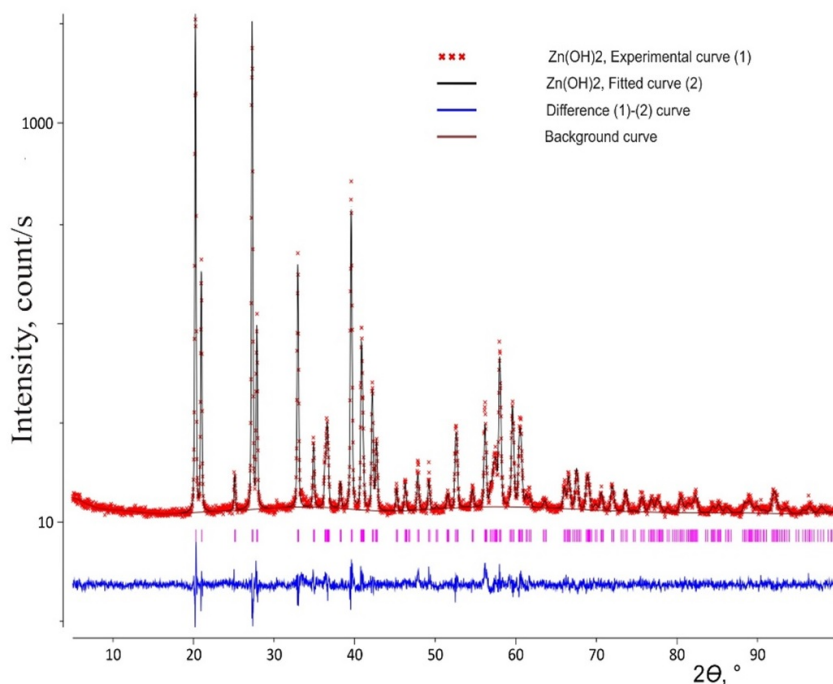
FIG. 3. Example of diffractogram of $Zn(OH)_2$ film (Wulfingit) on the glass substrate, which was performed on a STADI-P X-ray powder automatic diffractometer (STOE) with CuK$_{\alpha 1}$ radiation
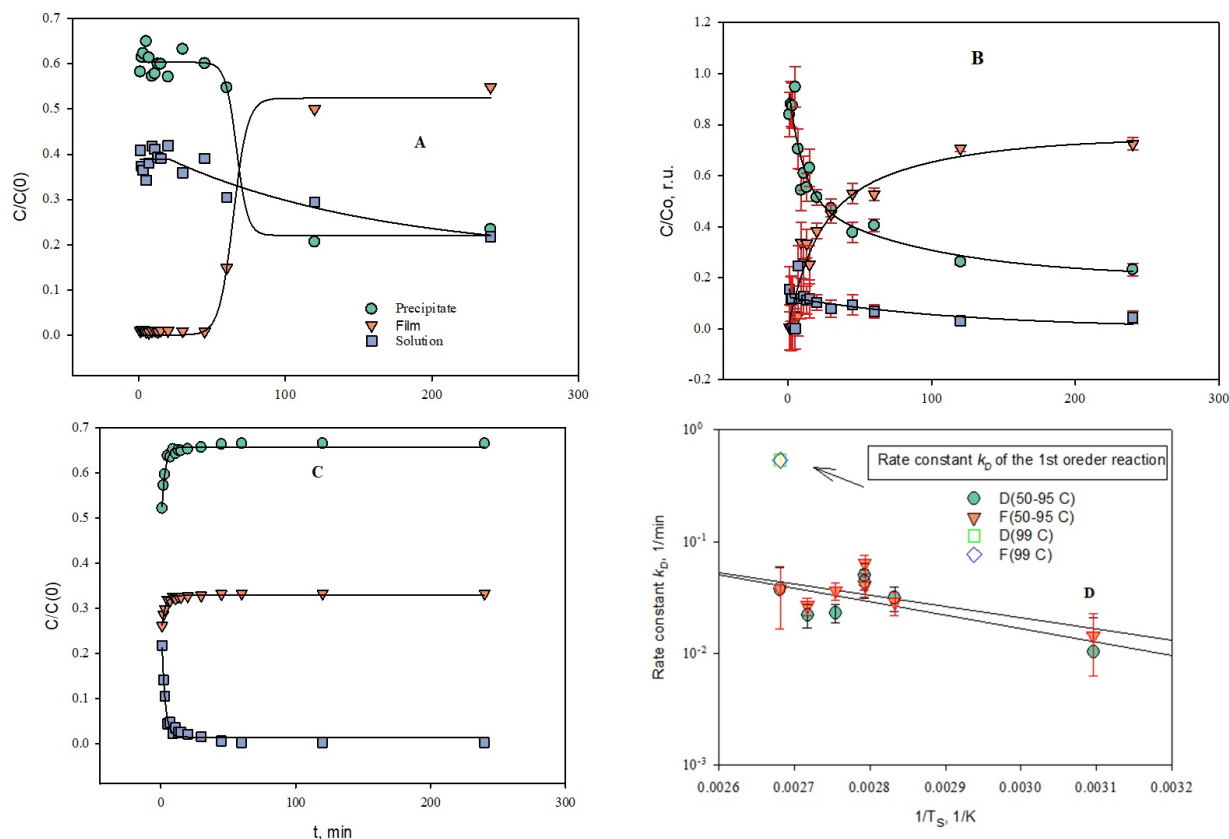
FIG. 4. Change of concentration of $Zn(OH)_2$, C/C(0) in the solution NH_3–$ZnAc_2$ versus the reaction time at different temperatures of the synthesis. C, C(0) are the current and initial concentration of zinc in the volume of the solution respectively. Synthesis temperature: (A) 50 °C, (B) 85 °C, (C) 99 °C. (D) the dependences of the rate constant (k_D) on T_s of the 1st order irreversible reaction of the disappearance of the sol (D) and the formation (F) of the film $Zn(OH)_2$–ZnO in the coordinates of the Arrhenius equation: the activation energies E_a of film growth (19±9) kJ/mol and of disappearance of the sol (23±10) kJ/mol. pH=10.3. The arrow shows the velocity constants at 99 °C

Thermodynamic analysis using the HSC Chemistry 8 program showed that the homogeneous state of the system (Σ) remains at a zinc concentration of 0.06 mol/l and a pH of 10.0 – 10.5 up to a temperature of 35 °C [35]. Further increase in the temperature creates supersaturation in the solution relative to the mixture of phases $Zn(OH)_2$ (Wulfingit)–ZnO (Zincite). As the temperature rises, the partial pressure of ammonia and water in the gas phase increases also. The concentration of ammonia dissolved in water changes little if at all. However, the partial pressure of the gases (primarily $H_2O(g)$, $NH_3(g)$) increases [38], and the colloidal phase of zinc hydroxide is formed. From the experimental data, it follows that the appearance of a colloidal solution is accompanied by the formation of zinc hydroxide particles of foamy morphology in the volume of the solution and on the surface of the walls of the glass reactor. The phase analysis of the films on the glass substrate and of the colloid particles, which was performed on a STADI-P X-ray powder automatic diffractometer (STOE) with CuK$_\alpha$ radiation, Fig. 3, has shown that due to the broadening of diffraction lines, they may be attributed to the presence of polycrystalline phases of Wulfingit and/or Zincite. These broadenings, Table 1, may be attributed to the presence of CSRs with a structure of $Zn(OH)_2$ and ZnO, as well as to distortions in their lattice [37].

We found the CSR sizes of the obtained films by using the Williams–Hall method for reflexes from the planes $\langle 001 \rangle$, $\langle 010 \rangle$, $\langle 001 \rangle$, $\langle 111 \rangle$ of the lattice of nanocrystals [37]. The width of the 90 % confidence interval of CSRs for this estimate varied within 2.7 nm for $Zn(OH)_2$ and 3.1 nm for ZnO, Table). It did not exceed 3 – 5 % of the CSR values of polycrystals in various diffraction planes. Since CSRs characterize the size of a single crystal region in the directions orthogonal to diffraction planes, the mean CSR value characterizes these single crystals as spherical particles at the 90 % confidence level regardless of their phase composition [39].

The Raman spectroscopy study of the samples of the $Zn(OH)_2$–ZnO films on the surface of the walls of a glass reactor was carried out at room temperature using a Via Reflex spectrometer, Renishaw (λ= 532 nm, P= 10 mW, exposure time 10 s). The samples were prepared in the following way: a test tube with a reaction solution was placed in a thermostat at a given synthesis temperature and was kept there for a sufficient time to complete the reaction of film formation on the walls of the tube and the formation of the $Zn(OH)_2$–ZnO precipitate at its bottom. The tube was then removed from
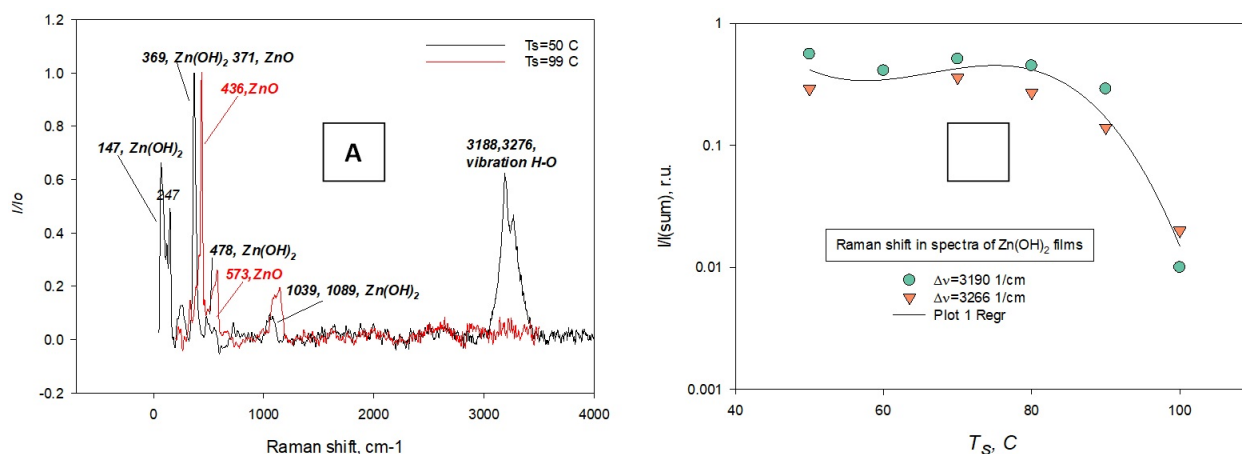
FIG. 5. (**A**) Examples of Raman spectra of Zn(OH)$_2$–ZnO film samples on the glass substrate, synthesized at temperatures T_s = 50 and 99 °C. I/I_0 – integral intensity (I) of the Raman band normalized to the highest bands intensity (I_o) in the spectrum. Identification of Raman shifts of Zn(OH)$_2$–ZnO is taken from [17]. (**B**) Changes in the relative intensity I/I_{sum} of vibration bonds of (OH)-groups belonging to Zn(OH)$_2$ films with temperature T_s in the Raman shift range from 3190 and to 3266 cm^{-1} according to Raman spectroscopy data. I_{sum} is the sum of all band's intensities in the spectrum range 0 – 4000 cm^{-1}. Regr – line of quadratic regression

the thermostat, the suspension was removed from the tube, the tube with the precipitated film was rinsed with water and dried at 23 °C until it became air-dry. After that, the test tube was fragmented. Fragments convenient for imaging the Raman spectrum were selected, and spectra were taken. The mass concentration of Zn(OH)$_2$–ZnO in the films (thickness) with the same composition of the solution changed little if at all, which made it possible to consider the geometry of the survey unchanged. The morphology of the ZnO layers on the substrate was studied on fragments prepared for Raman spectroscopy study by applying scanning electron microscopy (SEM) and EDX elemental analysis using a JSM JEOL 6390LA facility.

3. Experimental results

The results of analysis of the layers at the final stage of precipitation by SEM and EDX methods are presented in Fig. 2. One can see that the zinc hydroxide layer on the glass substrate is represented in the form of flower-like bunches of crystals with hexagonal section. The X-ray fluorescent spectrum of the layer reveals K_α and L_α lines of the principal elements Zn, O and minor lines of C, Si, Al which reflect the composition of the glass substrate. In the framework of thermodynamic analysis of the initially homogeneous system (Σ) we have refined our previous calculations using the HSC Chemistry 8 program. We included acetic acid (0.06 mol/l) and acetic complexes of Zn(II) in (Σ). The results showed that the homogeneous state of the system (Σ) remains at a zinc concentration of 0.06 mol/l and a pH of 10.0 – 10.5 up to a temperature of 35 °C and the concentration of Zn(CH$_3$COO)$_2$, Zn(Ac)$_2$ species in it two orders of magnitude lower than that of Zn(NH$_3$)$_4$(OH)$_2$, Fig. 1. The increase in the number and size of nanoparticles with temperature in the system (Σ) results in an increase in the ionic conductivity of the electrolyte solution due to the thermal decomposition of the ammonia complex Zn(NH$_3$)$_4$(OH)$_2$ followed by hydrolysis of ammonia molecules according to the scheme

$$\mathrm{Zn(NH_3)_4(OH)_2} \leftrightarrows \mathrm{Zn}^{2+}_{aq} + 4\mathrm{NH}_{3,aq} + 2\mathrm{OH}^-,$$

$$\mathrm{Zn}^{2+}_{aq} + 2\mathrm{OH}^- \to \mathrm{Zn(OH)}_{2,colloid}, \qquad (2)$$

$$\mathrm{NH}_{3,aq} + \mathrm{OH}^- \rightleftarrows \mathrm{NH_4OH} \leftrightarrows \mathrm{NH}_4^+ + \mathrm{OH}^-.$$
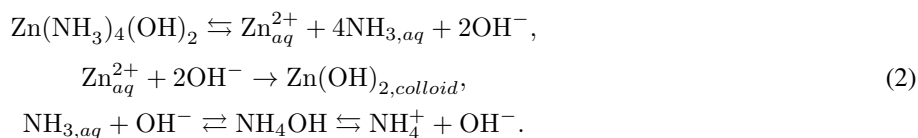
This leads to supersaturation relative to Zn(OH)$_2$, the formation of hydroxide particles in the form of colloidal clusters, and an increase in the concentration of ammonium ions in solution (2). The change in the concentration of Zn(II) ions in the reaction solution over the time of synthesis follows the equation of the irreversible reaction of the 1st order, (3), Fig. 4. The same relationship describes the change in the conductivity of the solution. As can be seen from Fig. 4, at $T_s = 50$ °C, the change in the concentration of particles in the film is characterized by an induction period. With an increase in temperature $T_s > 50$ °C, the duration of the induction period is reduced to zero, and the kinetics of film growth is determined by the loss rate of the number of colloidal nanocrystals in the solution due to the transfer of Zn(II) to the surface of the solution-reactor wall interface governed by an irreversible reaction of the 1st order.

The mean activation energy of the rate of colloid vanishing in solution and of the hydroxide film growth on the interface in this temperature range is E_a= (21±9) kJ/mol, Fig. 4D, [38]. At a temperature close to the boiling point of the electrolyte solution, the growth rate of the solid phase in the colloid system changes dramatically, Fig. 4C. Both processes
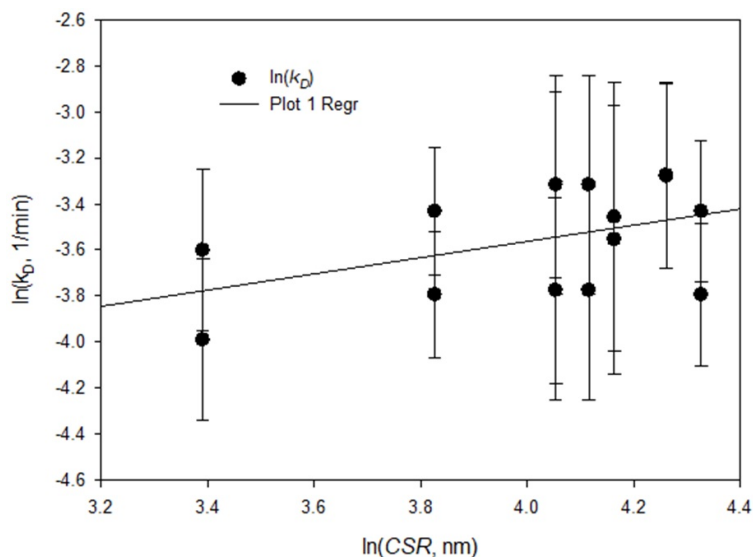
FIG. 6. Linear correlation between the mass growth (disappearance for the precipitate) rate constant $\ln(k_D)$ and $CSR \approx r$ for film and precipitate. The parameters of regression equation (4) estimated by the Least Square method are as follows: $b[0] = \ln(4\pi D) = -(5.00 \pm 0.75)$, $b[1] = x = (0.35 \pm 0.20)$
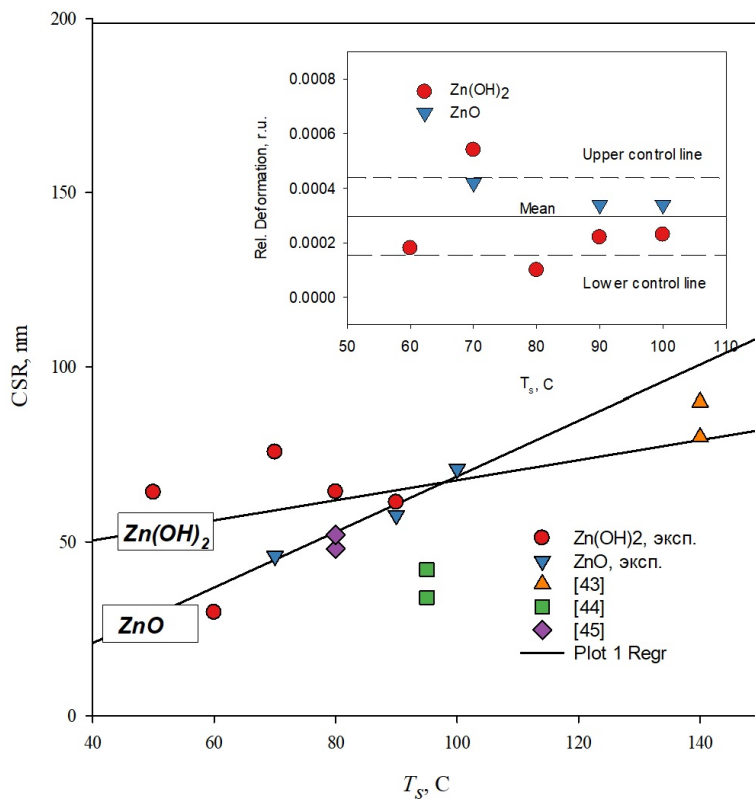
FIG. 7. Change in the mean value of the coherent scattering region (CSR) of Zn(OH)$_2$–ZnO nanocrystals in a film with synthesis temperature (T_s). The regression lines (Regr) characterize the change in the compared our experimental data. In square brackets next to the dot symbols, the numbers of available data sources [42–44] are shown, which are related to the CSR of ZnO according to the list of references. In the inset: the effect of the synthesis temperature on the mean relative deformation of nanocrystals in (001, 010, 001, 111) planes according to X-ray phase analysis data

of colloid and film growth begin to proceed in parallel at the same rate in accord with the first-order reaction relative to the concentration of Zn(II) ions.

Figure 5 shows typical Raman spectra of the $Zn(OH)_2$ film, which is formed on the glass substrate at $T_s = 55 - 95$ °C due to the thermal decomposition of the ammonia complex $Zn(NH_3)_4(OH)_2$ and hydrolysis of ammonia molecules according to scheme (2). We can see that the pure zinc oxide phase is formed at a temperature near the boiling point of the solution.

According to the classical theory of crystallization from a homogeneous solution, the initial stage of formation and growth of hydroxide/ oxide clusters is determined by the diffusion flow of ammonia complex $Zn(NH_3)_4(OH)_2$ to the surface of the growing cluster, the chemical reaction (2) of decomposition of the complex on the surfaces of the growing cluster, or by the mixed regime [18, 40, 41]. Under the conditions of $Zn(OH)_2$–ZnO clusters film growth at the surface of the reactor wall, a mixed growth mode is most likely. In that case, the monomer flux (J_D) to the growing cluster is related to the size of the growing cluster (r) by equation [40]:

$$J_D = \frac{dC}{dt} = -k_D(C - C_i), \quad k_D = 4\pi D r^x, \quad x = 1. \tag{3}$$

In (3), C and C_i are the concentrations of zinc ammonia complex in the volume of the solution and at the surface of the "cluster-solution" interface; k_D is the 1st order irreversible reaction rate coefficient for zinc ions measured in the experiment; and D is the diffusion coefficient. k_D depends on the current size of the cluster (r), which changes during growth and is a function of the concentration gradient ($C - C_i$). Therefore, the experimental dependence of k_D on the size of the cluster in the coordinates of equation (3) is of the form, in which the exponent (x) of the variable (r) characterizes the average value from zero to a maximum value of 1 or 2, depending on which mechanism of solid formation, diffusion growth and/or surface growth prevails. This conclusion follows from the results of comparison of the experimentally obtained relationship between the growth rate constant (k_D) and the CSR value, which we chose as an estimate of the average size of the critical cluster (r) in the film in the form of equation (4), Fig. 6,

$$\ln(k_D) = \ln(4\pi D) + x \ln(CSR) = b[0] + b[1]) \ln(CSR), \quad b[0] = n(4\pi D), \quad b[1] = x. \tag{4}$$

The mean value of exponent $b[1] = x = 0.35 \pm 0.20$ rel. units in equation (4) is close to, but less than unity, which does not contradict the diffusion or mixed diffusion model [41]. The diffusive nature of the cluster size growth is confirmed also by the coincidence of the determined activation energy of the film growth rate, $E_a = (21 \pm 9)$ kJ/mol, and the activation energy of diffusion of Zn(II) cations in the electrolyte solution (26 kJ/mol) [45].

The external diffusion transfer of Zn(II) ions to the surface of growing clusters in the form of the ammonia complex $Zn(NH_3)_4(OH)_2$ explains the observed first order of the film growth reaction for Zn(II) ions. At the same time, clusters tend to form aggregates and that proceeds to the growth of the film as a whole. The Raman spectra of the layers, which grow on the solution-glass walls interface, show that the hydroxide phase is the main phase in the T_s range $50 - 95$ °C, Fig. 5. According to the analysis of diffraction peak broadening, the polycrystalline film of the growing phase of $Zn(OH)_2$–ZnO is composed of spherical nanocrystals, the size of which is equal to the coherent scattering region, CSR [37]. The CSR depends on T_s, Fig. 7, but the crystal lattice parameters of the nanocrystals of both zinc hydroxide and oxide in the film composition remain constant across the entire range of T_s. Since the average value of the relative strain of nanocrystals of hydroxide and oxide phases in $\langle 001 \rangle$, $\langle 010 \rangle$, $\langle 001 \rangle$, $\langle 111 \rangle$ planes do not depend on the synthesis temperature T_s, Fig. 7 (inset), and does not exceed 0.04 %, the size factor can be considered to be the main reason for the observed widening of diffraction peaks [37].

The nanocrystals that make up the zinc hydroxide/oxide film have sizes (CSR) ranging from 20 to 60 nm, depending on the synthesis temperature, Fig. 7. From the point of view of the crystal growth theory [18], when the degree of supersaturation of the solution of $Zn(NH_3)_4(OH)_2$ changes with temperature, only those clusters are formed and remain stable that reach the critical size relative to the zinc hydroxide/oxide phase $\langle r \rangle$ [18, 19, 40]. The emergence of stable clusters of critical size opens a new route for colloid formation, consisting in the aggregation of these clusters. If the rate of aggregation of critical clusters significantly exceeds the rate of generation, the growing polycrystalline phase remains monodisperse, and the size of the nanocrystals corresponds to the size of the CSR observed in the experiment. With this exception, the schema of microcrystals formation at the final stage of the growth agrees well with the proposed earlier route of ZnO nanoflower growth [46, 47].

Let us analyze this hypothesis by applying the classical theory of crystallization as a model of the growing film of the $Zn(OH)_2$–ZnO composition. Let us represent the equilibrium solubility equation of nanocrystals (1) as (5), where the size of the critical cluster r is taken as an estimate of the size of the crystal $\langle r \rangle$

$$RT \ln(S/S_0) = \frac{\sigma \overline{V}}{\langle r \rangle}. \tag{5}$$

To assess the solubility of crystals (S, mol/l), we use the experimental values of the equilibrium concentration of zinc ions Zn(II) in a film synthesis solution at a given temperature T_s (equilibrium data for the "solution" curves, Fig. 4). The total concentration of zinc ions in the solution according to (5) depends on the degree of cation complexity in the

supernatant solution

$$\mathrm{Zn}_{aq}^{2+} + 4\mathrm{NH}_{3,aq} \rightleftarrows \mathrm{Zn(NH_3)}_4^{2+}, \quad \beta_4 = [\mathrm{Zn(NH_3)}_4^{2+}]/[\mathrm{Zn}_{aq}^{2+}][\mathrm{NH}_{3,aq}]^4. \tag{6}$$

To estimate the solubility, write the expression for S using reaction equations (6, 7) [18],

$$\mathrm{ZnO} + \mathrm{H_2O} \rightleftarrows \mathrm{Zn(OH)_2} \rightleftarrows \mathrm{Zn}_{aq}^{2+} + 2\mathrm{OH}_{aq}^{-}, \quad S = (SP_{ZnO}/2)^{1/3}, \quad S = [\mathrm{Zn}_{aq}^{2+}][= \mathrm{Zn(NH_3)}_4^{2+}]\beta_4[\mathrm{NH}_{3,aq}]^4, \tag{7}$$
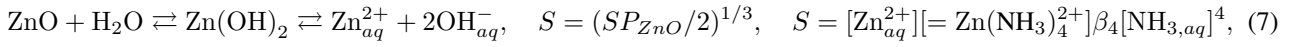
where SP is the solubility product of ZnO, and β_4 is the stability constant of the ammonia complex according to (6).

The peculiarity of using equation (7) to describe the experimental data for $\mathrm{Zn(OH)_2}$–ZnO nanoparticles is that their solubility is considered simultaneously as a function of the equilibrium temperature T_s and the size of the critical cluster $\langle r \rangle \sim CSR$:

$$\ln(S) = \ln(S_0) + \left(\frac{\sigma \overline{V}}{R}\right)\left(\frac{1}{T_s}\right)\left(\frac{1}{\langle r \rangle}\right) = \ln(S_0) + \left(\frac{\sigma \overline{V}}{R}\right)\left(\frac{1}{T_s} \times \frac{1}{CSR}\right). \tag{8}$$

Reaction (6) is shifted to the right under the conditions of the experiment. Therefore, the experimentally measured solubility at different synthesis temperatures (S) is determined by the concentration of the $\mathrm{Zn(NH_3)_4(OH)_2}$ complex. The term (S_0) in equation (6) characterizes the solubility component of single crystals $\mathrm{Zn(OH)_2}$–ZnO, which does not depend on T_s in the selected temperature range. We believe that in the considered temperature range the surface tension and molar volume of nanoparticles do not change significantly. Taking into account equation (7) and predominance of hydroxide in the T_s range 50 – 90 °C, Fig. 5, we cannot distinguish between impacts of ZnO and $\mathrm{Zn(OH)_2}$ phases on the solubility of the film as a whole. Thus, the experimental solubility (S) may be considered as a thermodynamic solubility of $\mathrm{Zn(OH)_2}$–ZnO films in the framework of equation (8).

The purpose of using the nanocrystal solubility equation (8) was to test the assumption that the CSR of the growing polycrystalline film does not differ from the size of the critical cluster $\langle r \rangle$ in the supernatant solution. To test this assumption, consider equation (8) in a form convenient for linear regression analysis (9):

$$\ln(S) = \ln([\mathrm{Zn}_{aq}^{2+}]) = \ln[\mathrm{Zn(NH_3)}_4^{2+}] - \ln(\beta_4[\mathrm{NH}_{3,aq}]^4) = \ln([\mathrm{Zn}_{aq}^{2+}]_0) + \left(\frac{\sigma \overline{V}}{R}\right)\left(\frac{1}{T_s}\right) \times \frac{1}{CSR}. \tag{9}$$

In (9), the independent variable (X) is the product of the inverse synthesis temperature T_s and the inverse value of the CSR:

$$\ln[\mathbf{Zn(NH_3)}_4^{2+}] = \ln([\mathrm{Zn}_{aq}^{2+}]_0) + \ln(\beta_4[\mathbf{NH}_{3,aq}]^4) + \left(\frac{\sigma \overline{V}}{R}\right)\left(\frac{1}{T_s} \times \frac{1}{CSR}\right),$$

$$Y = A + B \times X, \quad Y = \ln[\mathbf{Zn(NH_3)}_4^{2+}], \quad X = \left(\frac{1}{T_s} \times \frac{1}{CSR}\right), \tag{10}$$

$$A = \ln([\mathbf{Zn}_{aq}^{2+}]_0) + \ln(\beta_4[\mathbf{NH}_{3,aq}]^4), \quad B = \frac{\sigma \overline{V}}{R}.$$

Figure 7 also shows foreign literature data, in which the conditions of deposition of ZnO films from aqueous ammonia solution contain the information on T_s and the value of the oxide film CSR [42–44].

The experimental solubility of $\mathrm{Zn(OH)_2}$ and ZnO nanocrystals in the coordinates of equation (10) and the regression line $Y = A + B \times X$ based on the results of CSR analysis are shown in Fig. 8. It can be seen that the standard error in estimating the regression line, *Fit Std Err* = 1.10, is close to the error in estimating the concentration of Zn(II) ions in solution, (1.2 – 1.6) log. units. Therefore, equation (10) adequately describes the simultaneous effect of T_s and CSR on the solubility of $\mathrm{Zn(OH)_2}$–ZnO nanocrystals in the film composition. The value of CSR can be identified with the size of critically sized clusters $\langle r \rangle$, the aggregation of which ensures the growth of polycrystalline film by the mechanism of heteronucleation, facilitated by their low zeta potential.

From the data of Fig. 7 it can be seen that the size of CSR forming the film of hydroxide and zinc oxide depends differently on the synthesis temperature in the region of 50 – 95 °C. The CSR of hydroxide changes slightly in the entire region of its stability up to $T_s < 85 - 95$ °C. On the contrary, the CSR of oxide particles increases markedly with the growth of T_s.

If we extrapolate the $CSR(T_s)$ linear regression curve to the region of T_s=100 °C and above, we can see that with increasing T_s the $CSR(T_s)$ lines of hydroxide and zinc oxide intersect in the temperature zone of CSR= (50 – 100 nm). This size of CSR is comparable with the transverse dimensions of columnar microcrystals growing on the glass substrate (Fig. 2, inset). In this zone, we believe that the bulk growth speed of polycrystals from critical clusters in solution and the speed of parallel chemical reaction (2) on the surface of the fastest growing end face of hexagonal microcrystals become equal. The proposed change in the mechanism of high-temperature growth of ZnO microcrystals explain a sharp increase in the growth rate of the ZnO film and a visible transition to a parallel increase in the size of colloidal particles in solution and in film at 99 °C, Fig. 4C,D. Such interpretation is also consistent with the literature data [42–44, 47].
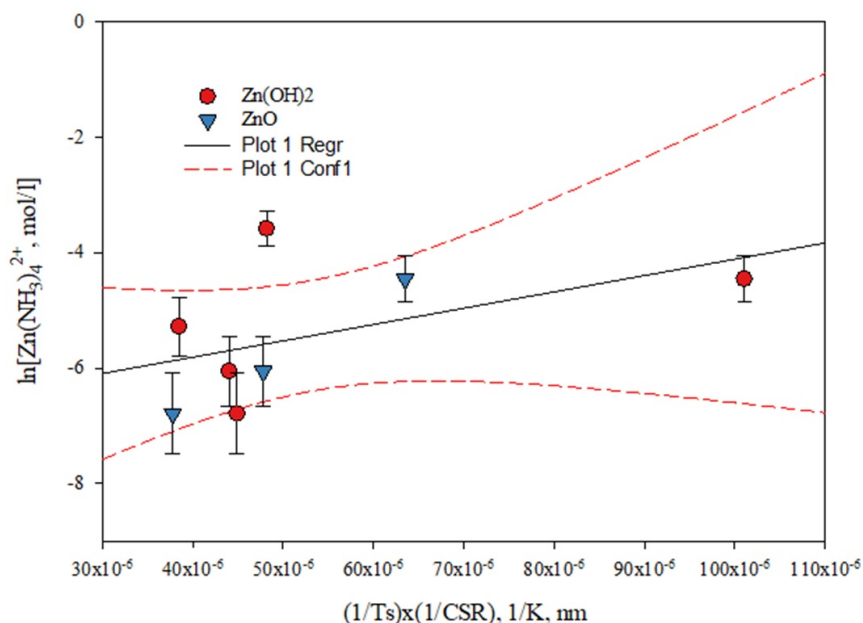
FIG. 8. Dependence of the molar solubility of zinc oxide in the system ($S \sim [\text{Zn(NH}_3)_4(\text{OH})_2]$) on the product of $(1/T_s) \times (1/CSR)$ in the coordinates of equation (10) according to the data on the equilibrium composition of the solution and film Zn(OH)_2–ZnO in 1 mol/l NH_3, pH=10.3. Parameters of the regression equation $Y = A + B \times X$, $A = (-6.90 \pm 1.10)$, $B = (2.80 \pm 2.00)10^4$, K, nm, *Fit Std Err*=1.10, F-value = 5. Regr – regression line, conf1 – 90 %-confidence intervals of regression

4. Conclusion

By using experimental methods of XRD, Raman spectroscopy, kinetic analysis along with thermodynamic modelling we have determined that the thermal impact on the dominated ammonia complex $\text{Zn(NH}_3)_4(\text{OH})_2$ in aqueous ammonia solutions leads to its decomposition, formation and growth of Zn(II) hydroxide/oxide clusters. According to the classical theory of crystallization from a homogeneous solution, this is a mixed process, the speed of which includes (i) – diffusion of ammonia complex $\text{Zn(NH}_3)_4(\text{OH})_2$ to the surface of the growing cluster and (ii) – the chemical reaction of decomposition of the complex on the surface of the cluster. The growth of Zn(OH)_2–ZnO clusters in solution and on the surface of the test tube glass is governed by the first order reaction regarding Zn(II). Process (i) prevails in the *Ts* range $50 - 95$ °C. At T_s= 99 °C, processes (i) and (ii) proceed in parallel at an order of magnitude higher speed.

The colloid-chemical mechanism of growth of Zn(OH)_2–ZnO clusters in solution and on the surface of glass substrate leads to the formation of microcrystals consisting of hydroxide/oxide nano-size clusters. Their average dimensions are equal to CSR of the microcrystals determined by the Williams-Hall method.

Relation (1) adequately describes the simultaneous effect of temperature *Ts* and CSR on the solubility of Zn(OH)_2–ZnO nanocrystals in the film composition. The value of CSR can be identified with the size of critically sized clusters, the aggregation of which ensures the growth of colloidal particles and their transfer to the polycrystalline film by the mechanism of heteronucleation. Such interpretation allows one to explain the microcrystalline morphology and monodisperse composition of the growing film.

Establishing of the picture of high-temperature colloid-chemical growth of ZnO layers from ammonia aqueous solutions in the T_s region above 100 °C in more details is a separate task, which requires further research.

References

[1] Mokrushin S.G. Experimental study of laminar systems. *Zhurnal Fizicheskoi Khimii (Journal of Physical Chemistry)*. 1934, 5(8), P. 1082–1091.

[2] Fabian I. Ezema, Chandrakant D. Lokhande, Rajan Jose, [Eds.]. *Chemically Deposited Nanocrystalline Metal Oxide Thin Films/Synthesis, Characterizations, and Applications*. Springer Cham., 2021, 926 p.

[3] Guire M.R.D., Bauermann L.P., Parikh H., Bill J. Chemical Bath Deposition. In: *Chemical Solution Deposition of Functional Oxide Thin Films*. [Eds.] Waser R., Kosec M., Payne D. Schneller T. Vienna, Springer, 2013, 350 p.

[4] Kozhevnikova N.S., Markov V.F., Maskaeva L.N. Chemical precipitation of metal sulfides from aqueous solutions: from thin films to colloidal particles. *Journal of Physical Chemistry*., 2020, **94**(12), P. 1752–1766.

[5] Maskaeva L.N., Markov V.F., Tulenin S.S., Forostyanaya N.A. *Hydrochemical Deposition of Thin Films of Chalcogenide Films: Practicum*. [Ed.] V.F. Markov. Ekaterinburg: M-vo obrazovaniya i nauki Ros. Federation, Urals. Feder. University, 284 p. (in Russian).

[6] Fatehah M.O. Hamidi A.A., Serge S. Stability of ZnO nanoparticles in solution. Influence of pH, dissolution, aggregation and disaggregation effects. *Journal of Colloid Science and Biotechnology*, 2014, **3**(1), P. 75–84.

[7] Majid A., Bibi M. Wet Chemical Synthesis Methods. In: *Cadmium based II-VI Semiconducting Nanomaterials*. Topics in Mining, Metallurgy and Materials Engineering. Cham. Springer, 2018.

[8] Guillemin S., Rapenne L., Roussel H., Sarigiannidou E., Brémond G., Consonni V.Formation Mechanisms of ZnO Nanowires: The Crucial Role of Crystal Orientation and Polarity. *Journal of Physical Chemistry C*, 2013, **117**(40), P. 20738–20745.

[9] He H., Lao C.S., Chen L.J., Davidovic D., Wang Z.L. Large-scale Ni-doped ZnO nanowire arrays and electrical and optical properties. *Journal of the American Chemical Society*, 2005, **127**, P. 16376–16377.

[10] Comini E., Faglia G., Sberveglieri G., Pan Z.W., Wang Z.L. Stable and high-sensitive gas sensors based on semiconducting oxide nanobelts. *Applied Physics Letters*, 2002, **81**, P. 1869–1871.

[11] He H., Hsin C.-L., Liu J., Chen L.J., Wang Z.L. Piezoelectric gated diode of a single ZnO nanowire. *Advance Materials*, 2007, **19**, P. 781–784.

[12] Sun X., Li Q., Jiang J., Mao Y. Morphology-tunable synthesis of ZnO nanoforest and its photoelectrochemical performance. *Nanoscale*, 2014, **6**(15), P. 8769–8780.

[13] Woo H.Y., Choi Y., Chung H. et al. Colloidal inorganic nano- and microparticles for passive daytime radiative cooling. *Nano Convergence*, 2023, **10**, P. 17–23.

[14] M. Li, L. Tonggu, X. Zhan, T.L. Mega, L. Wang. Cryo-EM Visualization of Nanobubbles in Aqueous Solutions. *Langmuir*, 2016, **32**(43), P. 11111–11115.

[15] Betenekov N.D., Medvedev V.P., Kitaev G.A. Deposition of cadmium sulfide films from solutions on the surface of glass. *Radiochemistry*, 1978, **20**(3), P. 431–438. (in Russian)

[16] Kitaev G.A. *Investigation of the Processes of Obtaining Metal Chalcogenide Films in Aqueous Solutions Containing Tio-, Selenourea and Sodium Selenosulfate*. Doctor thesis. Sverdlovsk, USSR : UPI afer S.M. Kirov, 1978. (in Russian)

[17] Lutz H.D., Jung C., Mortel R., Jacobs H., Stahl R. Hydrogen bonding in solid hydroxides with strongly polarizing metal ions, b-Be(OH)$_2$ and o-Zn(OH)$_2$. Spectrochimica Acta Part A, 1998, **54**, P. 893–901.

[18] Adamson A. *Physical Chemistry of Surfaces* (in Russian). [Eds.] B.V. Deryagin, Z.M. Zorin V.M. Muller. Moscow : Mir Publ., 1979, 568p

[19] Kapta G. The Gibbs Equation versus the Kelvin and the Gibbs-Thomson Equations to Describe Nucleation and Equilibrium of Nano-Materials. *Journal of Nanoscience and Nanotechnology*, 2011, **12**, P. 1-9.

[20] Gusarov V.V. The Role of Non-Autonomous Phases in the Transformations and Properties of Oxide Materials. [Ed.] N.V. Gelfond. Novosibirsk, INH SB RAS, 2023. Thermodynamics and Materials Science. Abstracts of the XV Symposium with international participation. June 3–5, 2023, P. 10.

[21] Polyakov E.V., Tzukanov R.R., Volkov I.V., Buldakova L.Yu., Baklanova I.V., Lipina O.A., Zhukov V.P., Kuznetsova Yu.V., Tutyunnik A.P., Maximova M.A. Synthesis and comparative photocatalytic activity of CuO layers on SiO$_2$ substrates. *Nanosystems: Physics, Chemistry, Mathematics*, 2020, **11**(5), P. 601–607.

[22] Polyakov E.V., Tsukanov R.R., Buldakova L.Yu., Kuznetsova Yu.V., Volkov I.V., Zhukov V.P., Maksimova M.A., Dmitriev A.V., Baklanova I.V., Lipina O.A., and Tyutyunnik A.P. Chemical Bath Precipitation and Properties of β-Ni(OH)$_2$ Films Prepared in Aqueous Ammoniac Solutions. *Russian Journal of Inorganic Chemistry*, 2002, **67**(6), P. 912–920.

[23] Le Pivert M., Martin N., Leprince-Wang Y. Hydrothermally grown ZnO nanostructures for water purification via photocatalysis. *Crystals*, 2022, **12**(308), P. 1–16.

[24] Pérez-Hernández R., Velázquez Salazar J.J., Yacaman M.J. Low-Temperature Synthesis and Growth Mechanism of ZnO Nanorods on Crystalline Si Substrate. *Journal of Nano Research*, 2011, **14**, P. 69–82.

[25] Wang M., Jiang L., Jung Kim E., Hahnc S.H. Electronic structure and optical properties of Zn(OH)$_2$: LDA+U calculations and intense yellow luminescence. *RSC Advances*, 2015, **5**, P. 87496–87503.

[26] Alnoor H., Chey Ch.O., Pozina G., Liu X., Khranovskyy V., Willander M., Nur O. Effect of precursor solutions stirring on deep level defects concentration and spatial distribution in low temperature aqueous chemical synthesis of zinc oxide nanorods. *AIP Advances*, 2015, **5**, P. 087180.

[27] Baviskar P.K., Nikam P.R., Gargote S.S., Ennaoui Ah., Sankapal B.RControlled synthesis of ZnO nanostructures with assorted morphologies via simple solution chemistry. *Journal of Alloys and Compounds*, 2013, **551**, P. 233–242.

[28] Znaidi L. Sol–gel-deposited ZnO thin films: A review. *Materials Science and Engineering: B*, 2010, **174**(1-3), P. 18–30.

[29] Polyakov E.V., Maksimova M.A., Kuznetsova Yu.V., Buldakova L.Yu. Colloidal-chemical mechanism of Zn(OH)$_2$–ZnO layer formation at the glass – ammonia solution – Zn(II) interface. *Nanosystems: Physics, Chemistry, Mathematics*, 2023, **14**(2), P. 231–241.

[30] Gonzalez-Chan I.J., Moguel Z.P., Oliva A.I. Deposition of ZnO thin films by chemical bath technique: physicochemical conditions and characterization. *ECS Journal of Solid State Science and Technology*, 2019, **8**(9), P. 536–544.

[31] Craig V.S.J., Krafft M.P.. Hot Topic – Nanobubbles and Nanodroplets Nanobubbles and Nanodroplets: from Basics to Applications. *Current Opinion in Colloid & Interface Science*, 2021, **55**, P. 101516.

[32] Xu-yu Zhang, Qian-shuai Wang, Zhong-xian Wu, Dong-ping Tao. An experimental study on size distribution and zeta potential of bulk cavitation nanobubbles. International Journal of Minerals, Metallurgy and Materials, 2020, **27**(2), P. 152–161.

[33] Kahraman S., Çakmak H.M., Çetinkaya S., Çetinkara H.A., Güder H.S. CBD grown ZnO nanostructures: effects of solution temperature. *International Journal of Materials Research*, (formerly Z. Metallkd.), 2013, **104**(8), P. 798–804.

[34] Trejo-Ramos A.I., Martín-Varguez P.E., Gonzalez-Chan I.J., Oliva A.I. Algorithm to obtain the species distribution diagrams and solubility curves for depositing ZnS, ZnO, and Zn(OH)$_2$ films in aqueous solution. Computational and Theoretical Chemistry, 2021, **1202**(113325), P. 1–8.

[35] Molefe F.V., Koao L.F., Dejene B.F., Swart H.C. Phase formation of hexagonal wurtzite ZnO through decomposition of Zn(OH)$_2$ at various growth temperatures using CBD method. *Optical Materials*, 2015, **46**, P. 292–298.

[36] Ki-Woong Chae, Qifeng Zhang, Jeong Seog Kim, Yoon-Ha Jeong, Guozhong Cao. Low-temperature solution growth of ZnO nanotube arrays. *Beilstein journal of nanotechnology*, 2010, **1**, P. 128–134.

[37] Williamson G., Hall W. X-ray line broadening from filed aluminium and wolfram. *Acta Metallurgica*, 1953, **1**, P. 22–31.

[38] Polyakov E.V., Maksimova M.A., Kuznetsova Y.V., Buldakova L.Y. Colloidal-chemical mechanism of growth of Zn(OH)$_2$–ZnO layers in the glass-ammonia solution interface Zn(II). OOO "GeLime", Proceeding of All-Russian Conference "Solid State Chemistry and Functional Materials-2022", XIV Symposium on Functional Materials. Ekaterinburg, 2022, P. 278–280. (in Russian)

[39] Balzar D. *Modeling of x-ray diffraction line broadening with the voigt function: applications to high-tc superconductors*. Colorado, National Institute of Standards and Technology, 1993, 87 p, NISTIR 3998.

[40] Thanh N.T.K. Maclean N. Mahiddine S. Mechanisms of Nucleation and Growth of Nanoparticles in Solution. *Chemical Reviews*, 2014, **114**, P. 7610–7630.

[41] Cheng J.J., Nicaise S.M., Berggren K.K., Gradečak S. Dimensional tailoring of hydrothermally-grown zinc oxide nanowire arrays. *Nano Letters*, 2016, **16**(1), P. 753–759.

[42] Lining Yang, Jing Wang, Lan Xiang. Hydrothermal synthesis of ZnO whiskers from e-Zn(OH)$_2$ in NaOH/Na$_2$SO$_4$ solution. *Particuology*, 2015, **19**, P. 113–117.

[43] Farhat O.F., Halim M.M., Abdullah M.J., Ali M.K.M., Allam N.K. Morphological and structural characterization of single-crystal ZnO nanorod arrays on flexible and non-flexible substrates. *Beilstein journal of nanotechnology*, 2015, **6**, P. 720–725.

[44] Koao L.F., Dejene F.B., Swart H.C. Properties of flower-like ZnO nanostructures synthesized using the chemical bath deposition. *Materials Science in Semiconductor Processing*, 2014, **27**, P. 33–34.

[45] Mamedova M.T. Kinetics and thermodynamics of Zn^{2+} ion sorption on the Na-form of catio-exchanger KB-4p-2. Actual Problems of the Humanities and Natural Sciences, 2012, 1. (in Russian)

[46] Acharyya D., Bhattacharyya P. An efficient BTX sensor based on ZnO nanoflowers grown by CBD method. *Solid-State Electronics*, 2015, **106**, P. 18–26.

[47] Lausecker C., Salem B., Baillin X., Consonni V. Modeling the elongation of nanowires grown by chemical bath deposition using a predictive approach. *Journal of Physical Chemistry C*, 2019, **123**, P. 29476–29483.

Information about the authors:

Maria A. Maksimova – ISSC UB RAS, 91, Pervomaiskaya str., 620108, Ekaterinburg, Russia; ORCID 0009-0004-2807-2222; msalimova1993@gmail.com

Evgeny V. Polyakov – ISSC UB RAS, 91, Pervomaiskaya str., 620108, Ekaterinburg, Russia; ORCID 0000-0001-7432-994X; polyakov@ihim.uran.ru

Ilya V. Volkov – ISSC UB RAS, 91, Pervomaiskaya str., 620108, Ekaterinburg, Russia; ORCID 0000-0001-8009-952X

Aleksandr P. Tyutyunnik – ISSC UB RAS, 91, Pervomaiskaya str., 620108, Ekaterinburg, Russia; ORCID 0000-0002-6394-4514

Alexey A. Ioshin – ISSC UB RAS, 91, Pervomaiskaya str., 620108, Ekaterinburg, Russia; ORCID 0009-0008-4679-1836; aaioshin@yandex.ru

Conflict of interest: the authors declare no conflict of interest.